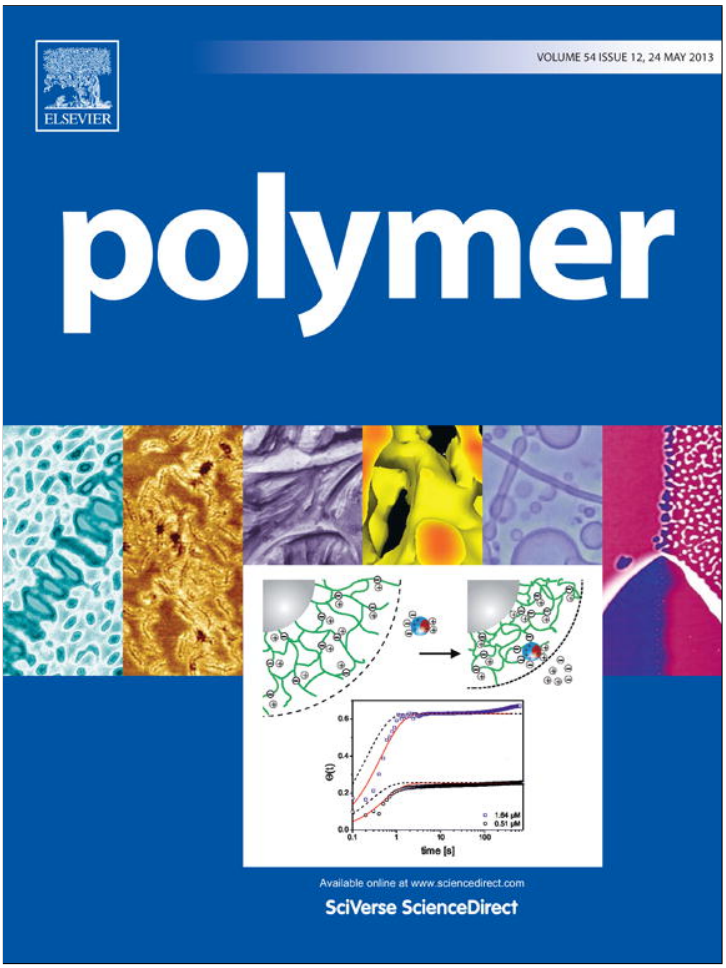

Polymer 54 (2013) 2952–2957

Contents lists available at SciVerse ScienceDirect

Polymer

journal homepage: www.elsevier.com/locate/polymer

Preparation and gas uptake of microporous organic polymers based on binaphthalene-containing spirocyclic tetraether

Mei-Yang Jiang [a,b], Qiu Wang [b,c], Qi Chen [b,**], Xin-Ming Hu [b], Xiao-Liang Ren [a,**], Zhong-Hua Li [c], Bao-Hang Han [b,*]

[a] College of Traditional Chinese Medicine, Tianjin University of Traditional Chinese Medicine, Tianjin 300193, China
[b] National Center for Nanoscience and Technology, Beijing 100190, China
[c] College of Chemistry, Central China Normal University, Wuhan 430079, China

ARTICLE INFO

Article history:
Received 24 December 2012
Received in revised form
28 March 2013
Accepted 1 April 2013
Available online 8 April 2013

Keywords:
Binaphthalene
Gas storage
Microporous polymers

ABSTRACT

Based on a spirocyclic tetraether derived from pentaerythritol and [1,1′-binaphthalene]-2,2′-diol, three porous organic polymers (**SPOP-7**∼**9**) were prepared through Suzuki reaction, Sonogashira–Hagihara reaction, and thiophene-based oxidative coupling polymerization, respectively. According to the obtained nitrogen physisorption isotherms, these polymers show permanent microporous nature with the Brunauer–Emmett–Teller specific surface area varying between 280 and 860 $m^2\ g^{-1}$. Uptake capacities of the polymers for gases (hydrogen and carbon dioxide) were also studied. Polymer **SPOP-9** prepared by oxidative coupling polymerization possesses the highest carbon dioxide adsorption capacity (12.6 wt %) among the three polymers at 1.0 bar and 273 K. Polymer **SPOP-7** shows moderate hydrogen adsorption capacity (1.43 wt %) at 1.0 bar and 77 K.

1. Introduction

Owing to the intrinsic properties of large surface area, narrow pore size distribution, high flexibility in the structure design, excellent thermal and chemical stability, and low skeleton density, porous organic polymers (POPs) have been studied extensively for potential applications, such as gas adsorption [1,2], membrane separations [3], organic electronic materials [4], and heterogeneous catalysis [5].

By selecting proper C–C coupling polymerization, versatile porous polymers could be obtained efficiently. For example, palladium-catalyzed Sonogashira–Hagihara coupling reaction and Suzuki coupling polymerization were usually used for preparation of porous poly(aryleneethynylene) and polyphenylene materials, respectively [6,7]. Nickel-promoted Yamamoto polymerization was used to synthesize microporous polymer materials [8], in which the polymerization can be performed with only a single monomer. Oxidative coupling polymerization catalyzed by $FeCl_3$ is also a reliable method to furnish porous polythiophene and polycarbazole materials [9,10].

Aromatic spirocyclic compounds, with the perpendicular arrangement structure of two planes, are novel core building units to produce contorted polymeric structures, which possess superior morphological stability. Due to the rigid and contorted structure, they have been employed as ideal building blocks in preparation of microporous polymers such as solution-processable polymers of intrinsic microporosity [11], conjugated microporous polymers with large specific surface area [10a,12], and microporous organic polymers with an exceptional uptake capacity for hydrogen [13]. Binaphthalene, as a core structural monomer for designing microporous organic polymers, has been used for preparation of conjugated microporous polymers [14], microporous soluble polyimide [15], and microporous heterogeneous catalysis [16]. Binaphthalene-based spirocyclic tetraether, possessing the binaphthalene rigid backbone and spirocycle contorted structure, has been used as a core structural monomer for designing microporous polymeric microsphere [17]. As for this spirocyclic monomer, the central $C(CH_2O-)_4$ unit has a slightly distorted tetrahedral geometry, where the $C-C_{core}-C$ angles range from 104.9(2)° to 111.9(2)°, and the geometry of monomer core is also controlled in part by distinctive short interannular C–H···O and C–H···π interactions [18]. Introducing a binaphthyl unit into conjugated polymer backbone can help manipulate the

* Corresponding author. Tel.: +86 10 8254 5576.
** Corresponding authors.
E-mail addresses: chenq@nanoctr.cn (Q. Chen), renxiaoliang@tjutcm.edu.cn (X.-L. Ren), hanbh@nanoctr.cn (B.-H. Han).

0032-3861/$ – see front matter © 2013 Elsevier Ltd. All rights reserved.
http://dx.doi.org/10.1016/j.polymer.2013.04.001

conjugation length of the polymer due to the tunable dihedral angle between two adjacent naphthalene rings in the binaphthyl unit [19], which provides an effective way to tailor the porous characteristics and improve the thermal or chemical stability of the obtained polymers [20]. In this article, preparation and gas storage properties of three types of POPs containing binaphthalene-based spirocyclic tetraether are reported. Binaphthalene-based spirocyclic tetraether has been proven as a good core structural monomer for designing microporous polymers with robust three-dimensional structures. Using the same core building monomer, the porosities and gas adsorption capacities of POPs can be controlled by varying the linkers and preparative methods. These polymers with the Brunauer–Emmet–Teller (BET) specific surface area varying between 280 and 860 $m^2\ g^{-1}$ show permanent microporous nature and moderate uptake capacities for hydrogen or carbon dioxide.

2. Experimental

2.1. Materials

All chemical reagents were commercially available and used as received unless otherwise stated. 1,4-Diethynylbenzene was purchased from Acros company. Thiophene-2-boronic acid and tetrakis(triphenylphosphine)palladium(0) were obtained from J&K company. **M-1** [18] and **M-3** [21] were prepared according to reported procedures, respectively.

2.2. Synthesis of *M-2*

M-1 (285.69 mg, 0.3 mmol) and thiophene-2-boronic acid (230 mg, 1.8 mmol) were dissolved in anhydrous *N*,*N*-dimethylformamide (DMF, 40 mL). After degassed by the freeze–pump–thaw cycles, to the mixture were added aqueous solution of potassium carbonate (2.0 M, 10 mL) and then tetrakis(triphenylphosphine) palladium(0) (30 mg, 33 μmol). The reaction mixture was stirred at 120 °C for 8 h under nitrogen atmosphere and monitored by TLC (v/v ethyl acetate:petroleum ether = 1:2). Then, the resulting mixture was cooled to room temperature, poured into water and extracted with ethyl acetate. The combined organic layer was dried over anhydrous sodium sulfate and concentrated under reduced pressure. The crude product was purified by column chromatography on silica gel (v/v ethyl acetate:petroleum ether = 1:4) to give the product **M-2** (280 mg, 96% yield) as a yellow solid. ^{1}H NMR (400 MHz, $CDCl_3$): δ (ppm) 8.13 (d, J = 1.6 Hz, 4 H), 8.10 (d, J = 1.6 Hz, 4 H), 8.02 (d, J = 8.8 Hz, 4 H), 7.92 (d, J = 9.2 Hz, 4 H), 7.55 (dd, J_1 = 2.0 Hz, J_2 = 8.8 Hz, 4 H), 7.51 (dd, J_1 = 1.6 Hz, J_2 = 8.8 Hz, 4 H), 7.22 (d, J = 8.8 Hz, 4 H), 7.11 (s, 4 H), 4.39 (d, J = 12.4 Hz, 8 H). MS (MALDI-TOF): *m*/*z* calculated for $C_{61}H_{40}O_4S_4$; 964.18 [M]; found: 964.17 $[M]^+$.

2.3. Synthesis of *SPOP-7* by Suzuki coupling polymerization

A solution of **M-1** (150.0 mg, 0.16 mmol) and **M-3** (97.6 mg, 0.2 mmol) in DMF (50 mL) was degassed by the freeze–pump–thaw cycles. To the mixture were added an aqueous solution of

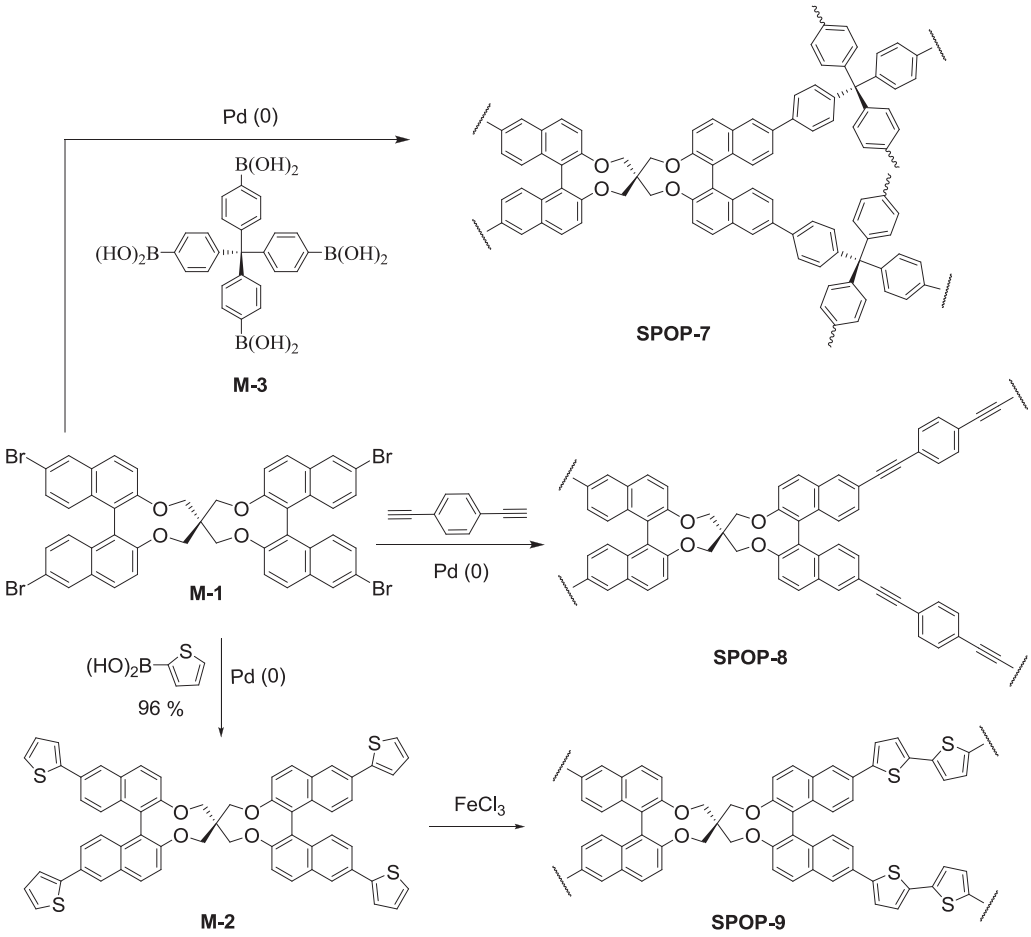

Scheme 1. Preparation of microporous polymers **SPOP-7 ~ 9**.

potassium carbonate (2.0 M, 10 mL) and then tetrakis(-triphenylphosphine)palladium(0) (30 mg, 33 μmol). The resulting solution was degassed and purged with nitrogen, and stirred at 150 °C for 24 h. The mixture was then cooled to room temperature and poured into water. The insoluble precipitate was filtered and washed with water, methanol, and acetone to remove any unreacted monomers or catalyst residues. Further purification of the polymer was carried out by Soxhlet extraction with water, methanol, and tetrahydrofuran (THF) for 24 h, respectively, to give **SPOP-7** (150 mg, 98%) as a black solid.

2.4. Synthesis of *SPOP-8* by Sonogashira–Hagihara coupling polymerization

A solution of **M-1** (133.3 mg, 0.14 mmol) and 1,4-diethynylbenzene (53.0 mg, 0.42 mmol) in DMF (25 mL) and triethylamine (25 mL) was degassed by the freeze–pump–thaw cycles. To the mixture was added tetrakis(triphenylphosphine)palladium(0) (30 mg, 33 μmol). The resulting solution was degassed and purged with nitrogen, and stirred at 90 °C overnight. The mixture was cooled to room temperature and poured into water. The precipitate was filtered and washed with water, methanol, and THF, respectively. Further purification of the polymer was carried out by Soxhlet extraction with water, methanol, and THF for 24 h, respectively, to give **SPOP-8** (110 mg, 90%) as a grey solid.

2.5. Synthesis of *SPOP-9* by thiophene-based oxidative coupling polymerization

M-2 (160 mg, 0.166 mmol) was dissolved in anhydrous chloroform (50 mL) and then the solution was added dropwise to a suspension of ferric chloride (216 mg, 1.328 mmol) in anhydrous chloroform (15 mL). The resulting mixture was stirred at room temperature overnight. Methanol (20 mL) was then added to the above reaction mixture, which was stirred for another hour. After collected by filtration, washed with methanol, and dried in air, the solid was collected and further stirred in 37% hydrochloric acid solution for 2 h. The suspension was then filtered and washed with methanol. The desired product was obtained (140 mg, 89%), after dried in vacuum oven at 70 °C overnight and further purification of the polymer by Soxhlet extraction with methanol, THF and dichloromethane for 24 h, respectively.

2.6. Instrumental characterization

The ^{1}H and ^{13}C NMR spectra were recorded on a Bruker DMX400 NMR spectrometer. Solid-state cross polarization magic angle spinning (CP/MAS) NMR spectra were recorded on a Bruker Avance III 400 NMR spectrometer. Mass spectra were recorded with a Microflex LRF MALDI-TOF mass spectrometer. Gas sorption isotherms were obtained with Micromeritics TriStar II3020 and Micromeritics ASAP 2020 M+C accelerated surface area and porosimetry analyzers at certain temperature. The samples were degassed *in vaccum* overnight at 120 °C. The obtained adsorption–desorption isotherms were evaluated to give the pore parameters, including BET specific surface area, pore size, and pore volume. The pore size distribution (PSD) was calculated from the adsorption branch with the nonlocal density function theory (NLDFT) approach. Scanning electron microscopy (SEM) observations were carried out using a Hitachi S-4800 microscope (Hitachi Ltd., Japan) at an accelerating voltage of 6.0 kV and equipped with a Horiba energy dispersive X-ray spectrometer. X-ray diffraction (XRD) patterns of the samples were acquired from 0.5 to 35° by a Philips X'Pert PRO X-ray diffraction instrument. The infrared (IR) spectra were recorded using a Perkin–Elmer Spectrum One FT-IR spectrometer.

3. Results and discussion

As shown in Scheme 1, three polymers were prepared via different polymerization methods. **SPOP-7** was obtained through Suzuki coupling polymerization between monomer **M-1** and **M-3**.

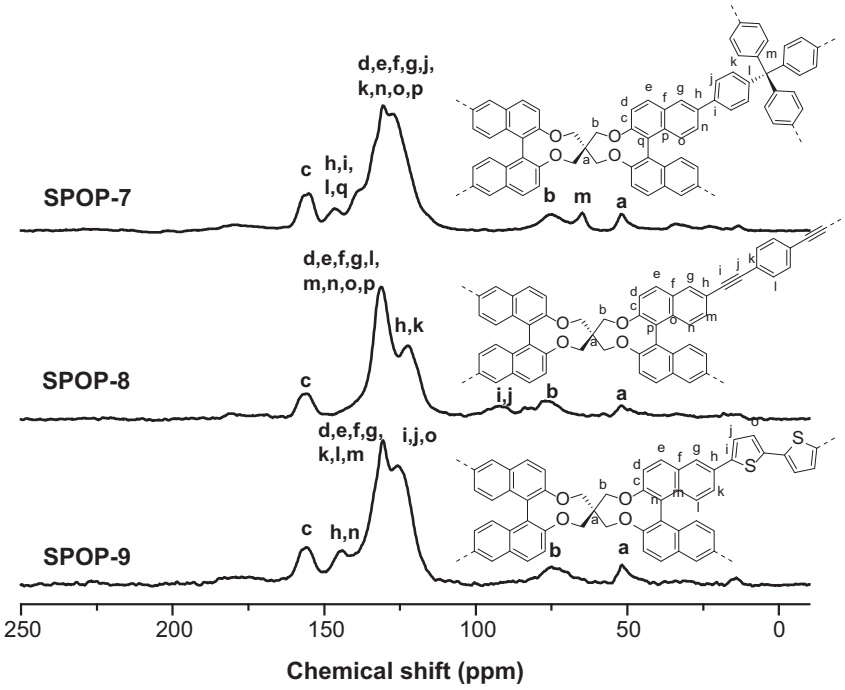

Fig. 1. ^{13}C CP/MAS NMR spectra of **SPOP-7**, **SPOP-8**, and **SPOP-9**.

SPOP-8 was prepared by Sonogashira–Hagihara coupling polymerization from **M-1** using 1,4-diethynylbenzene as the linker. Through thiophene-based oxidative coupling polymerization, **SPOP-9** was synthesized smoothly from **M-2** at room temperature, which can be obtained in quantitative yield by Suzuki coupling reaction between **M-1** and thiophene-2-boronic acid. All the polymers were obtained in high yields. Especially for **SPOP-7**, Suzuki coupling polymerization between monomer **M-1** and **M-3** can efficiently afford **SPOP-7** in the yield of 98%.

All obtained polymers were characterized at the molecular level by the solid-state ^{13}C CP/MAS NMR spectroscopy. The ^{13}C NMR spectra of the porous polymers with assignment of the resonances are shown in Fig. 1. All polymers show three similar peaks at about 155, 75, and 50 ppm, which are assigned to the substituted phenyl carbons binding with oxygen atom and alkyl carbons (methylene and quaternary carbons) in the spiro-cyclic moieties. As to **SPOP-7**, the peak at 65 ppm is ascribed to another quaternary carbon from **M-3**. The signal peak of –C≡C– of **SPOP-8** appears at about 92 ppm. For other aromatic carbons of the polymers, the signal intensities can be observed at the broad peaks range from 146 to 110 ppm. The structures of prepared polymers are also confirmed partly by their FT-IR spectra (Fig. S1, Supporting Information). Absorption peaks at about 3030 cm^{-1} (aromatic C–H stretching) and at nearly 1590–1460 cm^{-1} (C=C stretching bands) indicate the structure of aromatic ring. The signal peak that appears at about 1230 cm^{-1} corresponds to C–O–C stretching of the spiro-cycle containing oxygen atom. The absorption peak at around 2930 cm^{-1} is ascribed to the C–H stretching of methylene groups. All the above characterization data show that the desired polymers have been synthesized successfully.

The obtained POPs show an amorphous structure proved by XRD. Fig. S2 (Supporting Information) show the SEM images of the obtained polymers, respectively. They exhibit a similar morphology with different particle sizes. All the polymers are chemically stable, even exposed to dilute solution of acid or base, such as HCl or NaOH.

The porosity parameters of the polymers were studied by sorption analysis using nitrogen as the sorbate molecule. Nitrogen adsorption–desorption isotherms of **SPOP-7 ~ 9** measured at 77 K are shown in Fig. 2, in which the isotherms show rapid uptake at low relative pressure (P/P_0 = 0–0.1) indicating the microporous nature, especially for polymer **SPOP-9**. **SPOP-7** possesses a type I nitrogen gas sorption isotherm according to the IUPAC classification [22] and shows a very flat sorption plateau. The nitrogen isotherms for **SPOP-8** and **SPOP-9** differ substantially at the higher relative pressure range and exhibit a combination of type I and II nitrogen sorption isotherms. The isotherms show a continuous increase after the adsorption at low relative pressure, indicating an adsorption on the outer surface of small particles [23]. The increase in the nitrogen sorption at a high relative pressure above 0.9 may arise in part from interparticulate porosity associated with the meso- and macrostructures of the samples and interparticular void [24], especially for **SPOP-8**. In addition, hysteresis can be observed for the whole range of relative pressure based on the isotherms due to a linear increase of the adsorbed volume upon adsorption, which is attributed to the swelling in a flexible polymer framework induced by adsorbate molecules dissolved in nominally nonporous parts of the polymer matrix after filling of open and accessible voids [25] or the restricted access of adsorbate to the pores blocked by narrow openings, especially for non-ordered nanoporous materials [26].

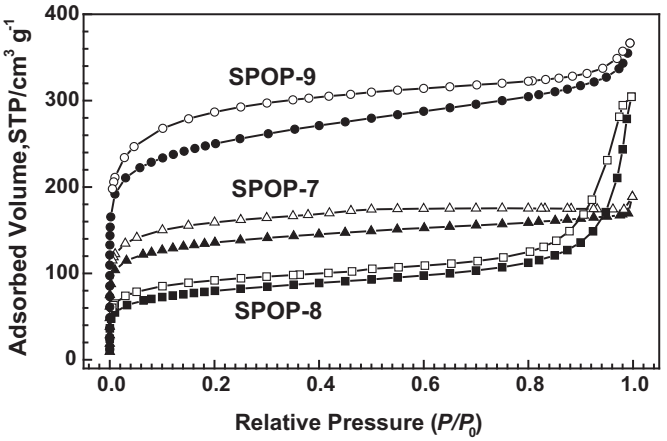

Fig. 2. Nitrogen adsorption–desorption isotherms of **SPOP-7**, **SPOP-8**, and **SPOP-9** measured at 77 K (adsorption branch is labeled with solid symbols and desorption is labeled with open symbols, respectively).

Listed in Table 1 are the key structural properties derived from the isotherm data such as BET and Langmuir specific surface area data, micropore specific surface area data, and pore volumes. The BET specific surface area values for these polymers range from 280 to 860 $m^2\ g^{-1}$, which are calculated in commonly used relative pressure (P/P_0) ranging from 0.05 to 0.2 (Fig. S3, Supporting Information). For the non-ordered porous materials, accurate determination of the PSD profile is very difficult. Different results are usually obtained according to different approaches. PSD analysis based on the NLDFT approach has been employed extensively to characterize a wide variety of porous materials although it does have limitations[25]. However, the calculated results can give some related qualitative information, with which one can make the relative comparison of materials synthesized by different monomers. The PSD profile of all polymers was calculated from the adsorption branch of the isotherms with the NLDFT approach. As shown in Fig. 3 and Table 1, the dominant pore sizes of **SPOP-7** and **SPOP-9** are centered at 0.59 and 0.62 nm, respectively. Polymer **SPOP-8** exhibits the similar PSD profile with dominant pore width at 0.59 and 0.67 nm. One common description to explain microporosity in amorphous polymers is that a homogeneous network model where the porosity is "molecular" in nature [27]. Porosities of polymers, such as the surface area and pore size, can be controlled by the monomer structure. For amorphous microporous polymers, it has been proven that the average micropore size and surface area can be fine-tuned in a continuous fashion with different monomer structures [6,13,28].

Porous polymers with a narrow pore distribution may interact attractively with small gas molecules through improved molecular

Table 1
Porosity properties and gas uptake capacities of polymers.

SPOP	S_{BET} ($m^2\ g^{-1}$)[a]	S_{micro} ($m^2\ g^{-1}$)[b]	V_{total} ($cm^3\ g^{-1}$)[c]	D_{pore} (nm)[d]	CO_2 uptake (wt %)[e]	H_2 uptake (wt %)[f]
SPOP-7	470 (620)	400	0.26	0.59	8.2	1.43
SPOP-8	280 (380)	120	0.33	0.59, 0.67	4.6	0.67
SPOP-9	860 (1150)	500	0.52	0.62	12.6	1.43

[a] Specific surface area calculated from the nitrogen adsorption isotherm using the BET method. The number in parentheses is the Langmuir specific surface area calculated from the nitrogen adsorption isotherm by application of the Langmuir equation.
[b] Micropore surface area calculated from the nitrogen adsorption isotherm using the *t*-plot method.
[c] Total pore volume at $P/P_0 = 0.97$.
[d] Data calculated from nitrogen adsorption isotherms with the NLDFT method.
[e] Data were obtained at 1.0 bar and 273 K.
[f] Data were obtained at 1.0 bar and 77 K.

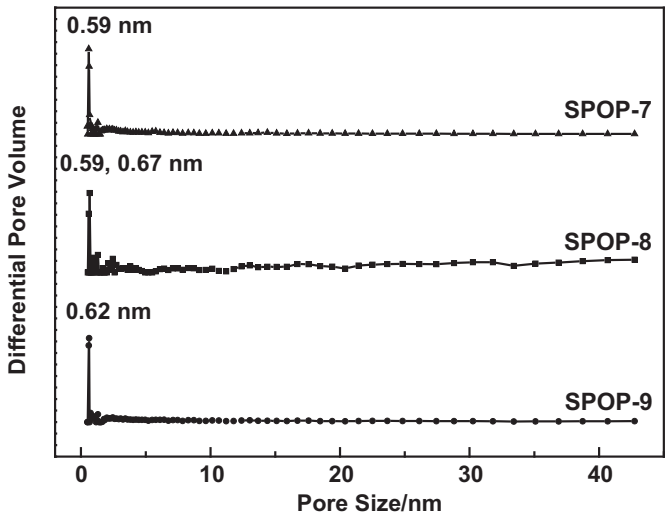

Fig. 3. PSD profiles calculated by NLDFT for **SPOP-7**, **SPOP-8**, and **SPOP-9**.

interaction. On account of the high capacity in hydrogen adsorption for many porous materials, we investigated the hydrogen uptake of **SPOP-7**∼**9** based on the hydrogen physisorption isotherms measured at 77 K and a pressure up to 1.13 bar (Fig. 4a). **SPOP-8**, possessing the lowest BET specific surface area ($S_{BET} = 280\ m^2\ g^{-1}$) and the lowest micropore specific surface area ($S_{BET} = 120\ m^2\ g^{-1}$) among the prepared polymers, exhibits the lowest hydrogen uptake of 0.67 wt % at 1.0 bar and 77 K. **SPOP-7** exhibits a same H_2 adsorption capacity (1.43 wt %) as **SPOP-9** at 1.0 bar and 77 K, even though the BET specific surface area of **SPOP-7** ($S_{BET} = 470\ m^2\ g^{-1}$) is much lower than that of **SPOP-9** ($S_{BET} = 860\ m^2\ g^{-1}$). Under the same conditions, the hydrogen uptake capacity of **SPOP-7** is comparable to some other porous polymers with a higher BET specific surface area [12,23,24].

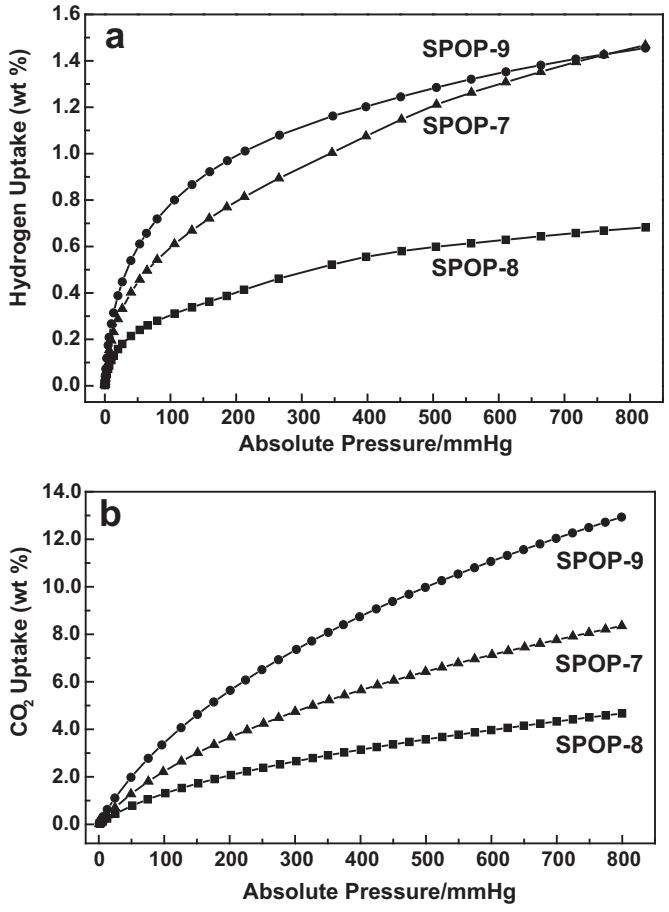

Fig. 4. a. Hydrogen adsorption isotherms of **SPOP-7**, **SPOP-8**, and **SPOP-9** at 77 K; b. CO_2 adsorption isotherms of **SPOP-7**, **SPOP-8**, and **SPOP-9** at 273 K.

From the hydrogen physisorption isotherm, we observed that **SPOP-7** seems to follow a linear increase in the uptake. Considering the relatively lower BET specific surface area of **SPOP-7** ($S_{BET} = 470\ m^2\ g^{-1}$), the hydrogen uptake for **SPOP-7** (1.43 wt % at 1.0 bar and 77 K) is unusually high. To investigate the impact of microporosity and the chemical nature of pore surfaces of **SPOP-7** on the hydrogen uptake, we further measured hydrogen adsorption isotherm of **SPOP-7** at 87 K (Fig. S4, Supporting Information) and calculated its isosteric heat of hydrogen adsorption based on adsorption isotherms at different temperatures (77 K and 87 K) from 0 to 1.13 bar through the Clausius–Clapeyron equation [9]. As shown in Fig. 5, it can be observed that the isosteric heat of **SPOP-7** is about 6.2 kJ mol^{-1} at zero coverage. The isosteric heat value is higher than that for some other porous polymer analogs, such as PAF-1 (4.6 kJ mol^{-1}) [8b], PPN-3 (5.5 kJ mol^{-1}) [29], and polyimide network PI-1 (5.3 kJ mol^{-1}) [30]. The higher heat of adsorption implies that the presence of enhanced affinity between hydrogen molecules and **SPOP-7**. In addition, compared their BET specific surface areas (5600 $m^2\ g^{-1}$ for PAF-1, 2840 $m^2\ g^{-1}$ for PPN-3, and 1407 $m^2\ g^{-1}$ for polyimide network PI-1) and hydrogen adsorption capacities (∼1.50 wt % for PAF-1, 1.58 wt % for PPN-3, and ∼1.30 wt % for polyimide network PI-1 at 1.0 bar and 77 K) with those of **SPOP-7**, we can see that specific surface area is not the only criterion for hydrogen adsorption.

The uptake capacity of polymers for carbon dioxide was also studied. From the carbon dioxide physisorption isotherms measured at 273 K and a pressure up to 1.13 bar (Fig. 4b). It could be found that an increase trend in the carbon dioxide loading capacity with increasing specific surface area (Table 1). **SPOP-9**, possessing the highest BET specific surface area among the prepared polymers, exhibits the uptake capacity of 12.6 wt % for carbon dioxide at 1.0 bar and 273 K. Compared with **SPOP-7** and **SPOP-8**, the higher carbon dioxide loading capacity of **SPOP-9** might be attributed to its higher charge density at the sulfur sites of networks that can facilitate local-dipole/quadrupole interactions with carbon dioxide [31].

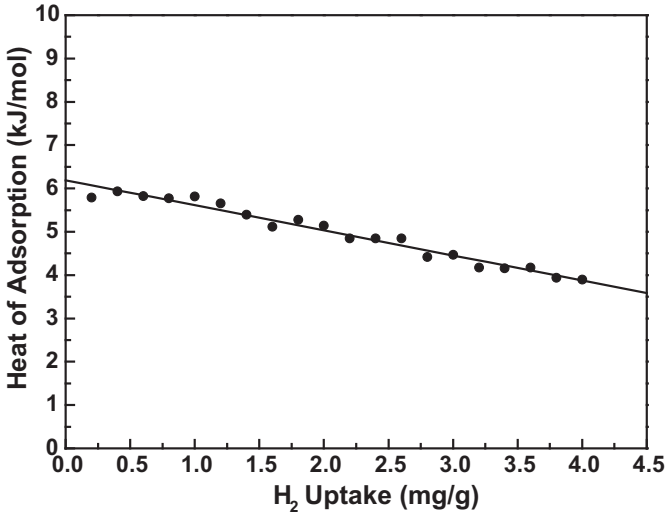

Fig. 5. Isosteric heat of hydrogen adsorption for **SPOP-7**.

4. Conclusions

In summary, based on the spirocyclic tetraether derived from pentaerythritol and [1,1′-binaphthalene]-2,2′-diol, three porous organic polymers have been synthesized by different types of C–C coupling polymerization. The BET specific surface area for these polymers is up to 860 $m^2\ g^{-1}$. **SPOP-7** exhibits a similar H_2 adsorption capacity (1.43 wt % at 1.0 bar and 77 K) to **SPOP-9**, even though the BET specific surface area of **SPOP-7** ($S_{BET} = 470\ m^2\ g^{-1}$) is much lower than that of **SPOP-9** ($S_{BET} = 860\ m^2\ g^{-1}$). **SPOP-9**, possessing the highest BET specific surface area among the prepared polymers, exhibits the uptake capacity of 12.6 wt % for carbon dioxide at 1.0 bar and 273 K. Using the same core building monomer, the porosities and gas adsorption capacities of porous organic polymers can be tuned by varying the linkers. Binaphthalene-containing porous polymers have a promising performance for gas storage, gas-selective adsorption, and heterogeneous catalysis.

Acknowledgments

The financial support of National Science Foundation of China (Grants 91023001, 61261130092, and 21274033) and the Chinese Academy of Sciences (Grant KJCX2-YW-H21) is acknowledged.

Appendix A. Supplementary data

Supplementary data related to this article can be found at http://dx.doi.org/10.1016/j.polymer.2013.04.001.

References

[1] a) Morris RE, Wheatley PS. Angew Chem Int Ed 2008;47:4966–81;
b) Wu D, Xu F, Sun B, Fu R, He H, Matyjaszewski K. Chem Rev 2012;112:3959–4015.
[2] a) Thomas A. Angew Chem Int Ed 2010;49:8328–44;
b) Dawson R, Cooper AI, Adams DJ. Prog Polym Sci 2012;37:530–63.
[3] Wind JD, Staudt-Bickel C, Paul DR, Koros WJ. Ind Eng Chem Res 2002;41:6139–48.
[4] Wan S, Guo J, Kim J, Ihee H, Jiang D. Angew Chem Int Ed 2008;47:8826–30.
[5] a) Mackintosh HJ, Budd PM, McKeown NB. J Mater Chem 2008;18:573–8;
b) Kaur P, Hupp JT, Nguyen SBT. ACS Catal 2011;1:819–35.
[6] a) Jiang J-X, Su F, Trewin A, Wood CD, Campbell NL, Niu H, et al. Angew Chem Int Ed 2007;46:8574–8;
b) Jiang JX, Su F, Trewin A, Wood CD, Niu H, Jones JTA, et al. J Am Chem Soc 2008;130:7710–20.
[7] a) Weber J, Thomas A. J Am Chem Soc 2008;130:6334–5;
b) Chen Q, Luo M, Wang T, Wang J-X, Zhou D, Han Y, et al. Macromolecules 2011;44:5573–7.
[8] a) Schmidt J, Werner M, Thomas A. Macromolecules 2009;42:4426–9;
b) Ben T, Ren H, Ma S, Cao D, Lan J, Jing X, et al. Angew Chem Int Ed 2009;48:9457–60.
[9] Chen Q, Luo M, Hammershøj P, Han Y, Laursen BW, Yan C-G, et al. J Am Chem Soc 2012;134:6084–7.
[10] a) Yuan S, Kirklin S, Dorney B, Liu D-J, Yu L-P. Macromolecules 2009;42:1554–9;
b) Schmidt J, Weber J, Epping JD, Antonietti M, Thomas A. Adv Mater 2009;21:702–5.
[11] Budd PM, Elabas ES, Ghanem BS, Makhseed S, McKeown NB, Msayib K, et al. Adv Mater 2004;16:456–9.
[12] Jiang JX, Laybourn A, Clowes R, Khimyak YZ, Bacsa J, Higgins SJ, et al. Macromolecules 2010;43:7577–82.
[13] Chen Q, Wang JX, Wang Q, Bian N, Li ZH, Han B-H. Macromolecules 2011;44:7987–93.
[14] Dawson R, Laybourn A, Clowes R, Khimyak YZ, Adams DJ, Cooper AI. Macromolecules 2009;42:8809–16.
[15] a) Ritter N, Antonietti M, Thomas A, Senkovska I, Kaskel S, Weber J. Macromolecules 2009;42:8017–20;
b) Ritter N, Senkovska I, Kaskel S, Weber J. Macromol Rapid Commun 2011;32:438–43.
[16] Kundu DS, Schmidt J, Bleschke C, Thomas A, Blechert S. Angew Chem Int Ed 2012;51:5456–9. Angew Chem 2012; 124: 5552–5.
[17] Chen Q, Wang Q, Luo M, Mao LJ, Yan CG, Li ZH, et al. Polymer 2012;53:2032–7.
[18] Tu T, Maris T, Wuest JD. J Org Chem 2008;73:5255–63.
[19] Zheng L, Urian RC, Liu Y, Jen AK-Y, Pu L. Chem Mater 2000;12:13–5.
[20] Zhang C, Hua C, Wang G, Ouyang M, Ma C. Electrochim Acta 2010;55:4103–11.
[21] Fournier JH, Maris T, Wuest JD, Guo W, Galoppini E. J Am Chem Soc 2007;125:1002–6.
[22] Sing KSW, Everett DH, Haul RAW, Moscou L, Pierotti RA, Rouquérol J, et al. Pure Appl Chem 1985;57:603–19.
[23] Rose M, Klein N, Böhlmann W, Böhringer B, Fichtner S, Kaskel S. Soft Mater 2010;6:3918–23.
[24] Chen Q, Wang J-X, Yang F, Zhou D, Bian N, Zhang X-J, et al. J Mater Chem 2011;21:13554–60.
[25] Weber J, Schmidt J, Thomas A, Böhlmann W. Langmuir 2010;26:15650–6.
[26] Rose M, Böhlmann W, Sabo M, Kaskel S. Chem Commun 2008;44:2462–4.
[27] Wood CD, Tan B, Trewin A, Niu H, Bradshaw D, Rosseinsky MJ, et al. Chem Mater 2007;19:2034–48.
[28] Yuan S, Dorney B, White D, Kirklin S, Zapol P, Yu L, et al. Chem Commun 2010;46:4547–9.
[29] Lu W, Yuan D, Zhao D, Schilling CI, Plietzsch O, Muller T, et al. Chem Mater 2010;22:5964–72.
[30] Wang Z, Zhang B, Yu H, Sun L, Jiao C, Liu W. Chem Commun 2010;46:7030–2.
[31] Farha OK, Spokoyny AM, Hauser BG, Bae YS, Brown SE, Snurr RQ, et al. Chem Mater 2009;21:3033–5.